Journal of Marine Research, 73, 17–32, 2015

Distinguishing turbulent overturns in high-sampling-rate moored thermistor string observations

by Hans van Haren[1] and Louis Gostiaux[2]

ABSTRACT

Turbulent overturns are distinguished from salinity-compensated intrusions in high-resolution moored thermistor string observations. The buoyancy frequency N is used to make the time dimensionless, "t^*." This results in a primary, visual means to easily compare the duration of overturns with N, the natural frequency that separates internal waves from turbulent overturns. As a secondary means, the shapes of overturns are investigated. Above various sloping topography between 500 and 1,000 m water depth where the buoyancy period varies between ∼1,300 and 2,600 s, vertical overturns of ∼40 m last $\Delta t^* = 0.2-0.4$. This corresponds with the timescale of growth of model-stratified turbulence in the wake of a grid. Smaller-scale, weaker-turbulent, shear-induced Kelvin-Helmholtz overturns of ∼5 m are observed to last approximately $\Delta t^* = 0.03$, whereas the passage of their train of multiple consecutive overturns lasts up to approximately $\Delta t^* = 0.95$. Although the shape of overturns can distinguish salinity-compensated intrusions from turbulent overturns, the present observations from internal wave breaking above sloping topography show complex results of mixed features.

Keywords. Turbulent overturn patterns, high-resolution temperature observations, detailed ocean mixing parameter estimates, salinity-compensated intrusions

1. Introduction

High-resolution depth-time series from thermistor strings moored above sloping underwater topography reveal large turbulent overturns exceeding 40 m in height (e.g., van Haren and Gostiaux 2012). These overturns are associated with internal wave breaking, and most vigorous ones have been found associated with upslope moving frontal bores. The precision of the thermistors ($<5 \times 10^{-4}$ °C) and the resolution in the vertical and in time, ∼1 m and 1 s, respectively, are potentially adequate to estimate turbulence parameter values using overturn reordering (Thorpe 1977). Such estimates can be made undisputedly from thermistor string observations in lakes, where temperature (T) dominates density variations. In seas and oceans, one has to verify the contribution of salinity (S) to density anomaly

1. Royal Netherlands Institute for Sea Research (NIOZ), P.O. Box 59, 1790 AB Den Burg, The Netherlands. ***e-mail: hans.van.haren@nioz.nl***

2. Laboratoire de Mécanique des Fluides et d'Acoustique, UMR CNRS 5509, École Centrale de Lyon, Université de Lyon, 36 avenue Guy de Collongue, 69134 Écully cedex, France.

variations ($\delta\sigma_p$) at a given pressure (depth). This can be done practically using one or more shipborne conductivity-temperature-depth (CTD) profiles near the mooring.

In areas where a "tight" mean linear relationship is found between T and S, or actually between variations δT and $\delta\sigma_p$, turbulence parameters can be estimated from moored thermistor string data. Because a few CTD profiles cannot monitor the δT-$\delta\sigma_p$ relationship in detail over the mooring period, care is taken to recognize small and large layers of temperature inversions ("intrusions") that might be (over-)compensated by salinity as these give false, nonturbulent overturning information. Van Haren and Greinert (2013) postulate that intrusions are relatively easy to distinguish visually in detailed turbulence parameter images from thermistor string data. One distinction is the rapid variation over four orders of magnitude from genuine turbulent overturns to quiescent periods in between. In contrast, intrusions maintain high "false-overturn" levels for prolonged periods of time, as, for example, around Mediterranean outflow lenses in the Atlantic Ocean and the spreading of dense water at its compensation depth following convective formation. Both can persist for days to months. Despite potential contamination as a result of intrusions, it is advantageous to use temperature-only data because moored salinity observations are profoundly difficult to make and will yield at least 10 times higher noise levels in density variations, which makes adequate estimates of turbulence parameters perhaps even more difficult.

In the present article, we elaborate on this approach to better distinguish effects of intrusions in moored T-only turbulence parameter estimates. The scaling of time using the local buoyancy frequency is useful to quantify the ocean turbulent overturn duration. The buoyancy frequency separates turbulence from internal waves (e.g., Gregg 1987), and model-grid-stratified turbulence is observed to halt its growth after one-quarter buoyancy period (Riley, Metcalf, and Weissman 1981; Itsweire, Helland, and Van Atta 1986).

Such numerical and experimental laboratory turbulence data are compared here with deep-ocean moored observations, where the typical depth-time-mean buoyancy period $T_{<[N]>} = 2\pi/<[N]> \approx 1{,}500$ s. The moored observations have some similarity with towed near-surface high-sampling rate thermistor string observations (e.g., Dugan 1984; Marmorino 1987). These observations in the highly stratified thermocline show individual overturns that extend diapycnally across some 10 m vertically and 100 m horizontally. In the less stratified deep ocean, the aspect ratio of overturns will tend to unity; hence, the typical duration of "frozen" overturns in Eulerian measurements should not exceed $\Delta t = \Delta z/\bar{u}$ (Taylor hypothesis), where Δz is the vertical extent of the overturn, and $\bar{u}$ the mean horizontal velocity. With typical values of Δz = 10 m and $\bar{u} = 0.1$ m s^{-1} (van Haren and Gostiaux 2012; van Haren and Greinert 2013), this maximum duration is one order of magnitude smaller than $T_{<[N]>}$.

2. Data

High-sampling-rate Royal Netherlands Institute for Sea Research (NIOZ) self-contained temperature sensors were moored at various locations above sloping topography (positions

will be given in Section 4). Arbitrarily, the depth interval was chosen between 500 and 1,000 m, the bottom slopes not being critical for internal tidal waves (van Haren and Gostiaux 2012; van Haren and Greinert 2013). The sampling rate was always 1 Hz, with precision better than 5×10^{-4} °C and a noise level of 6×10^{-5} °C. NIOZ3 (van Haren et al. 2009), NIOZ4, or NIOZ4c sensors were used. NIOZ4 (including tilt sensor) and NIOZ4c (including compass sensor) are upgrades of NIOZ3, with similar characteristics, except for their reduced size (two-thirds smaller) and reduced power consumption (with the capacity of sampling at a rate of 1 Hz for the duration of 1.5 years). The sensors are synchronized via induction every 4 hours, so that the timing mismatch is smaller than 0.02 s.

Temperature sensor data are converted to conservative (approximately potential) temperature (Θ) values (McDougall et al. 2009) to compensate compressibility effects before they are used as a tracer for potential density variations. A constant $\delta\Theta$-$\delta\sigma_p$ relationship is obtained from linear best-fit data using nearby CTD profiles across at least twice the vertical range of thermistors. This relationship provides an indication of the variability of water mass properties over the large vertical ($\Delta z = \sim$100 m) buoyancy scales. The number $O(100)$ of sensors and their vertical resolution of $\sim$1 m are sufficient to resolve the small buoyancy scales. Thus, the thermistor string data can be used to estimate turbulence parameters, especially in areas where internal waves break (van Haren and Gostiaux 2012). These estimates are not made via resolution of the smallest Kolmogorov scales $O(10^{-3}-10^{-2})$ m of turbulence dissipation, as in microstructure profiler data, but through resolution of scales of up to the largest energy-containing Ozmidov scales of turbulence in stratified fluids.

The turbulent kinetic energy dissipation rate, $\varepsilon = 0.64d^2N^3$, and vertical (z) turbulent eddy diffusivity, $K_z = 0.128d^2N$, are estimated by calculating "overturning" displacement scales (d) after reordering every 1 Hz time step of the potential density (temperature) profile, which may contain inversions, into a stable monotonic profile without inversions (Thorpe 1977, 1987). The displacement of each parcel of fluid is assigned to its depth in the (stable) source profile as in van Haren and Gostiaux (2012, 2014), and thus not to its depth in the (unstable) observed profile as in Thorpe (1977). The displacement is chosen to be positive when the water parcel moves upward from the (unstable) observed profile to reach its depth in the (stable) source profile, as in van Haren and Gostiaux (2014). This convention of sign has no effect on the turbulence parameter estimates, which are based on d^2. It is noted that the opposite sign convention was used in previous publications of the authors (e.g., van Haren and Gostiaux 2012). N denotes the local buoyancy frequency of the reordered density profile, and a constant mixing efficiency of 0.2 is used (Osborn 1980; Oakey 1982). As the instrumental noise is very low, and given the moderate but still substantial stratification in the examples presented here, all detected overturns exceed the threshold commonly used for detecting overturns (Stansfield, Garrett, and Dewey 2001; van Haren et al. 2009; van Haren and Gostiaux 2012).

The particular shape of overturns in the d-z plane is used as a secondary means to distinguish genuine turbulent overturns from "false" overturns attributable to intrusions. Details have been described for CTD observations by van Haren and Gostiaux (2014).

They show that a slope of $z/d = 0.5$ can be modeled by a solid body overturn, whereas a Rankine vortex has slopes $0.5 < z/d < 1$ in the shape's interior and just exceeding $z/d = 1$ along the sides. A homogeneous mixed layer with noise added fills a parallelogram with a long axis exactly sloping $z/d = 0.5$ and sides $z/d = 1$. An intrusion model gives slopes $z/d >> 1$.

In the following, averaging over time is denoted by [. . .], and averaging over depth range by $< \ldots >$. The specific averaging periods and ranges are indicated with the mean values.

3. Scaling time

Besides using the shape of overturns in the d-z plane, we use another (visual) means to investigate ocean turbulent overturns and to separate the effects of salinity compensation from moored temperature observations. We extend the practice in turbulence investigations in which, for a constant N, dimensionless time Nt is used (e.g., Itsweire, Helland, and Van Atta 1986) for the case of a time-varying N. Thereby, we scale the time axis of the temperature sensor data in integral form with the instantaneous depth-range-mean buoyancy frequency $[N](t)$, so that we arrive at the dimensionless parameter,

$$t^* = \int_{\text{period}} [N](t)/2\pi \, dt, \tag{1}$$

in which "period" denotes the entire time interval of the figure depicted. A dimensionless time interval, $\Delta t^* = 1$, corresponds in real time to one depth-time-mean buoyancy period, $T_{<[N]>}$.

As seen in the example of Figure 1, the effect of the scaled time is that periods with weakly stratified waters, like before the front, become shortened horizontally, and that strongly stratified periods, like after the front, become elongated horizontally (compare Fig. 1a, the original time axis, with Fig. 1b, the t^*-axis; the delay between the two is given in Fig. 1d).

The grid width of one unit (t^*) is useful for separation in ocean dynamics because motions with periodicities longer than this bar will be mainly internal waves, whereas motions shorter than it will be mainly turbulent overturns (Gregg 1987). A rudimentary form of this scaling is given in the Appendix. Thus, potentially for the duration of $t^* < 1$ an overturn can remain statically unstable, although numerical modeling by Riley, Metcalf, and Weissman (1981) suggested that the turbulence already collapses at $Nt \approx \pi/2$ (see Gregg 1987), which corresponds to $t^* = 0.25$. As a side effect of equation (1), a weak dynamic influence can be seen by comparing the original (Fig. 1a) with the scaled (Fig. 1b) data. Nonlinear portions like fronts have a slightly more linear appearance in the latter.

As salinity-compensated intrusions have no dynamic constraint, they can have timescales longer or shorter than one unit. They are relatively easily detected when they last for $\Delta t^* > 1$ (see examples in Section 4; none were detected in Fig. 1). However, intrusions are also relatively easily detected when they last for $\Delta t^* < 1$ because of their particular layering and flattening of the turbulence parameter estimates (see Section 4).

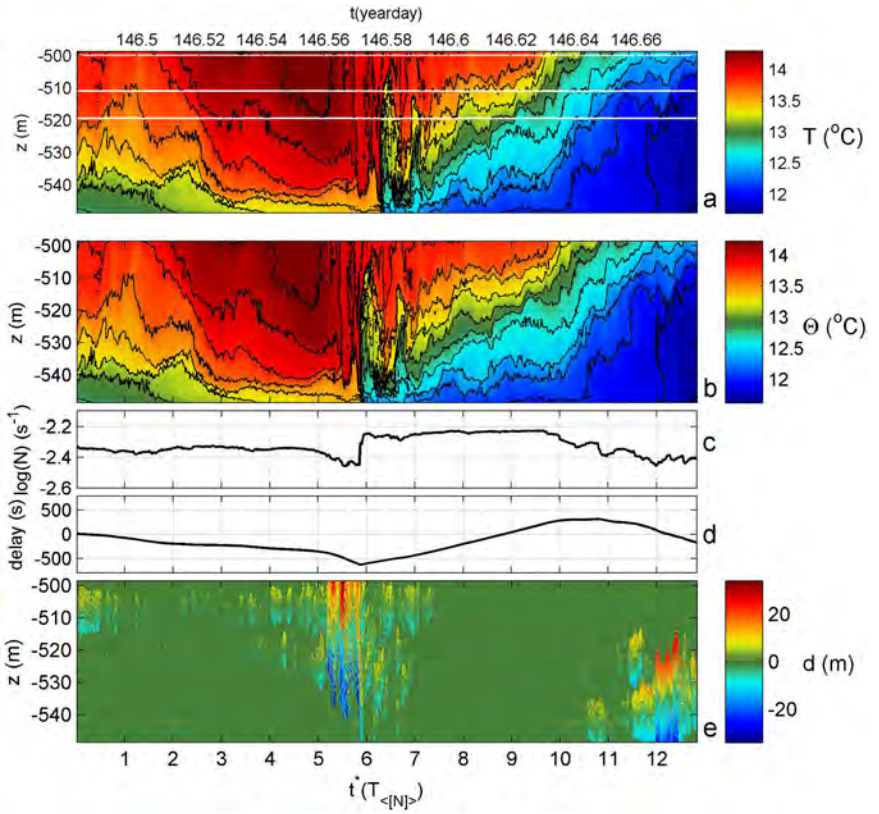

Figure 1. The effect of t^*, equation (1), time scaled with the vertical mean $[N](t)$ per $\Delta t = 1$ s temperature profile, for a sample period of 4.8 hours above Great Meteor Seamount (100 NIOZ3 sensors at 0.5 m intervals, between 0.5 and 50.0 m above the bottom). (a) Depth-time series of original temperature data, with time in yeardays. Black contours are drawn every 0.2°C. (b–e) The t^* series: (b) As in panel (a), but for conservative temperature without contours shifted by -0.076°C and missing data (three sensors) interpolated. Any duration of overturn displacements shorter than one unit of t^* is considered not an internal wave and is potentially turbulence. Any longer, they are "false" overturns. (c) Vertically averaged buoyancy frequency computed from the reordered profiles of panel (b). (d) Delay between t^* rescaled with depth-time-mean buoyancy frequency and time t. This indicates the shrinking (decreasing delay) and stretching (increasing delay) in time. (e) Depth-t^* series of displacements necessary to obtain the reordered profiles.

4. Observations of genuine and false overturns

a. Wave breaking in an area with tight T-S relationship

As reported in van Haren and Gostiaux (2012) for observations at 250 m below the underwater summit of Great Meteor Seamount (30.0° N, 28.3° W; 549 m water depth), the T-S relationship, and thus $\delta\sigma_p = \alpha\delta\Theta$, is reasonably tight: $\alpha = -0.101 \pm 0.002$

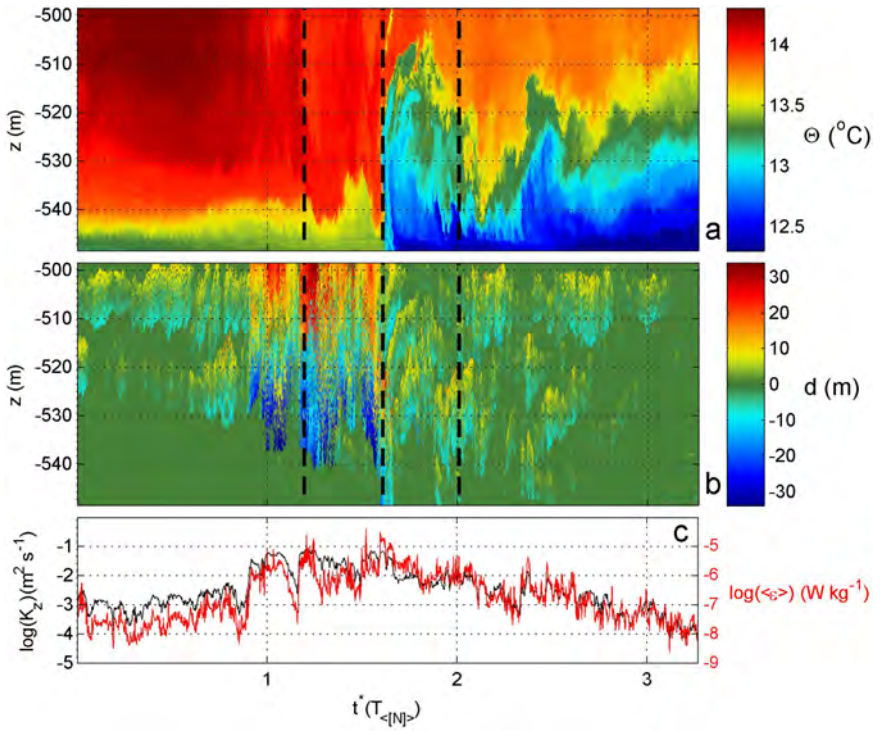

Figure 2. Overturn-duration investigation around the passage of a front above Great Meteor Seamount in a 1.2-hour detail between days [146.55, 146.60] as a function of t^*. (a) Conservative temperature. (b) Displacements after reordering. (c) The t^* series of vertically averaged eddy diffusivity (black) and dissipation rate (red, scale to the right). The vertical dashed lines refer to t^*'s of displacement profiles in Figure 3.

kg m^{-3} °C^{-1} represents the thermal expansion coefficient under local conditions. This area is well above the 1,000–1,500 m depth range of Mediterranean outflow in the northeast Atlantic Ocean. Repeated nearby CTD observations show very little variation in the relationship previously described, and the effects of intrusions are thus expected to be negligible.

Nevertheless, in a detail view around a frontal bore passage, some large, vertical instabilities of alternating slightly warmer and cooler columns of water are observed around the left dashed line in Figure 2(a). Because these instabilities are observed just prior to a (frontal) change from the warming downslope moving phase of the internal tide to the cooling upward moving phase, they may be associated with oblique internal wave propagation over the seamount. Such oblique propagation can generate instabilities over a slope (Gemmrich and van Haren 2001). As can be seen in Figure 2(b) and (c), the associated large overturns are all of short duration ($\Delta t^* << 1$) when measured between delimiter values of

1% of the local maximum values. The latter are $[K_z] \approx 3 \times 10^{-2}$ m^2 s^{-1}, $[\varepsilon] \approx 10^{-6}$ W kg^{-1} (m^2 s^{-3}), in this case. A precise value of Δt^* for overturns cannot be given because of the considerable variability.

The values between $0.2 < \Delta t^* < 0.4$ are typical for large overturns ($|d| > 10$ m); see also further before and well after the frontal passage. This duration corresponds with model results for turbulence in the wake of a grid and for which the growth stops at $t^* \approx 0.25$ (Riley, Metcalf, and Weissman 1981; Itsweire, Helland, and Van Atta 1986).

After the front passage, just to the right of the rightmost dashed line in Figure 2(a), vertical instability motions of relatively warm water are observed having about the same duration as the large instabilities before the arrival of the front. Clearly, the 50 m range of thermistors is insufficient to resolve all of the large near-bottom turbulence above Great Meteor Seamount. This was already concluded from the unresolved tidal amplitude, which was estimated to measure 100 m top to trough (van Haren and Gostiaux 2012). The turbulent overturns extending upward of the thermistor range were previously thought to be part of high-frequency internal waves. Measured in terms of t^*, they are more likely part of the frontal overturning system. Only further after the frontal passage do the large ones turn into linear internal waves (cf. rightmost third of Fig. 1b, especially around the light-blue layer).

Examples of the shape of a detail of large overturns corresponding to the dashed lines in Figure 2 are given in Figure 3, in which 10 consecutive profiles are used in each panel. It is seen that the borders of these overturns all more or less align with a slope of 1 in the d-z plane, indicated by the dashed lines of the background grid. The solid lines of the background grid have a slope of 0.5. The overturn cores of these 10 profiles (blue circles) are quite erratic, as are those in their average profiles (red asterisks). However, in smaller pieces of $\sim$5 m vertical extent, the core slopes are $\sim$0.5–0.7 in the d-z plane. This value range is typical for complex genuine turbulent overturns, in this case best modeled by a Rankine vortex (van Haren and Gostiaux 2014). Recall that false overturns due to intrusions would have slopes well larger than 1.

Genuine turbulence is certainly expected for a train of classic roll-up overturns in Kelvin-Helmholtz (K-H) billows (Fig. 4 between $[-540, -530]$ m; van Haren and Gostiaux 2010). Indeed, the billows have a timescale of $\Delta t^* \approx 0.03 << 1$. This short timescale is consistent with the billows' relatively small vertical extent of typically 5 m. It results in relatively weak turbulent exchange, which is two orders of magnitude smaller than in Figure 2. In contrast with the duration of the individual billows, the passage of the entire train of consecutive billows in Figure 4 lasts $\Delta t^* = 0.95 \pm 0.05$.

Despite the relatively small turbulence parameter values associated with K-H billows, the variation with time of these values is still considerable and exceeds two orders of magnitude. In Figure 4, the grid width of $1t^*$ is about equal to the length of the smallest free propagating internal waves, which are visible in the yellow upper part of Figure 4(a). Besides the train of K-H billows, Figure 4 shows multiple other overturns of approximately one to two times the size of K-H in t^*-z. These are thus also much smaller than the grid width and can be considered as genuine turbulent overturns. This may be concluded after inspection of the

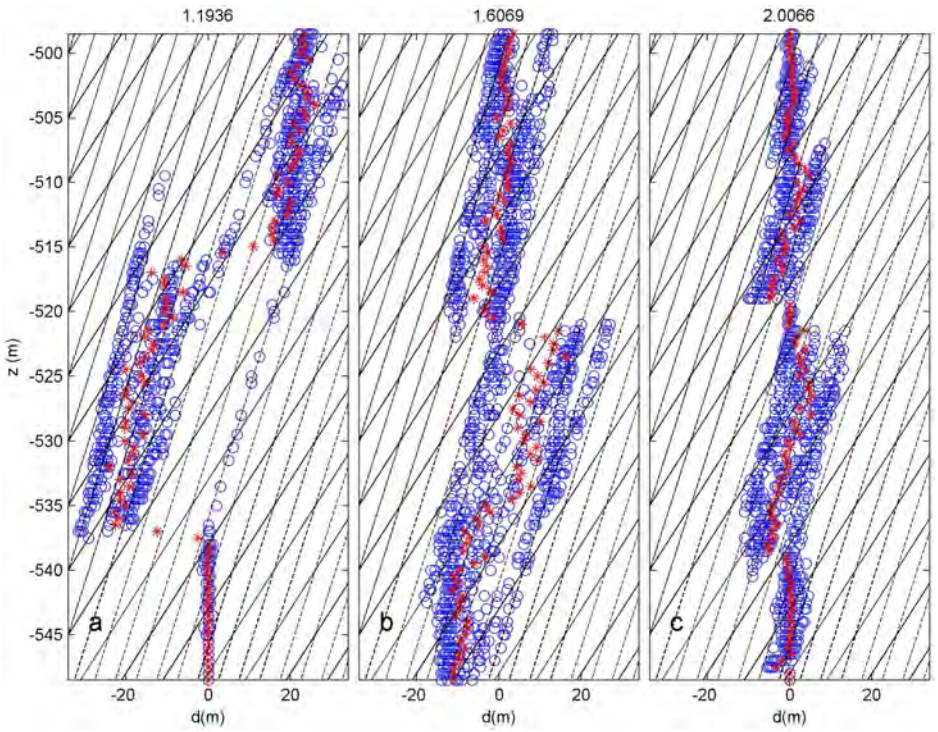

Figure 3. Ten consecutive profiles of displacements (blue circles) and their mean values at given depths (red asterisks) for t^*'s indicated above and along dashed lines in Figure 2. The grid consists of two slopes in the d-z plane: 0.5 (solid lines) and 1 (dashed lines).

shape of overturns (Fig. 5). The K-H billows are the largest overturns in Figure 5(b) and (c). The data points of the overturns form parallelograms in the d-z plane, with sloping side edges and horizontal borders at top and bottom and very similar to a model of a fully mixed overturn (van Haren and Gostiaux 2014). Their sloping edges are aligned with $z/d = 1$, whereas their cores, in one or two layers, and their long axis align nearly perfectly with $z/d = 0.5$. This is also observed for all other overturns in Figure 5.

b. Areas with varying intrusions

Strong intrusions have been observed during the first 2 out of 5 days of data above a sloping side of Opouawe Bank off New Zealand (41.7° S, 175.5° E; 969 m water depth; van Haren and Greinert 2013); see the example in Figure 6. In the t^*-z plane, intrusions are characterized by thin (∼5 m vertical extent; e.g., crossing the middle dashed line) or thick (∼40 m vertical extent; e.g., crossing the leftmost dashed line) layers of apparent overturns.

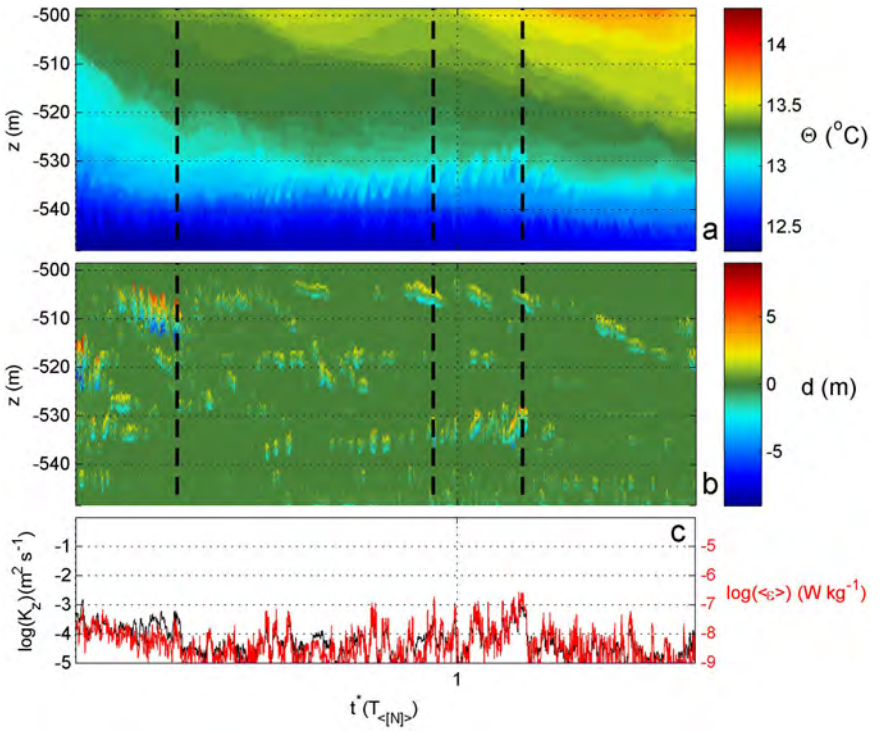

Figure 4. Overturn-duration investigation for 0.6 hours between days [143.86, 143.885] of Great Meteor Seamount data during the passage of a train of Kelvin-Helmholtz overturns between $-540 < z < -530$ m. Note that the turbulence parameter values are $\sim$100 times smaller given the same buoyancy period compared with Figure 2. This shows in the scale change in panel(b).

These layers are moved up and down by internal wave motions, but they retain their height and displacements, and thus turbulence parameter values, more or less persistently over $\Delta t^* > 1$. As a result, they have the character of false overturns, and the turbulence parameter estimates are not genuine. It is noted that their turbulence estimates vary over less than one order of magnitude, as measured in isotherm-internal wave following coordinates.

Superposed on the intrusion layer of large vertical extent are high-frequency fluctuations. Because they have a duration of $\Delta t^* \approx 0.04 << 1$, they cannot be internal waves; they have a duration of slightly (30%) longer than that of the K-H billows discussed previously, in an area where the buoyancy period is twice as long. They extend over a 10-fold larger vertical range than the K-H discussed previously. As a result, the intrusions are found to be vertically intersected by genuine turbulent overturns, probably because salinity is merely just compensating temperature so that the layer of 40 m thick is near homogeneous in density. The latter is confirmed by CTD profiles taken before mooring deployment.

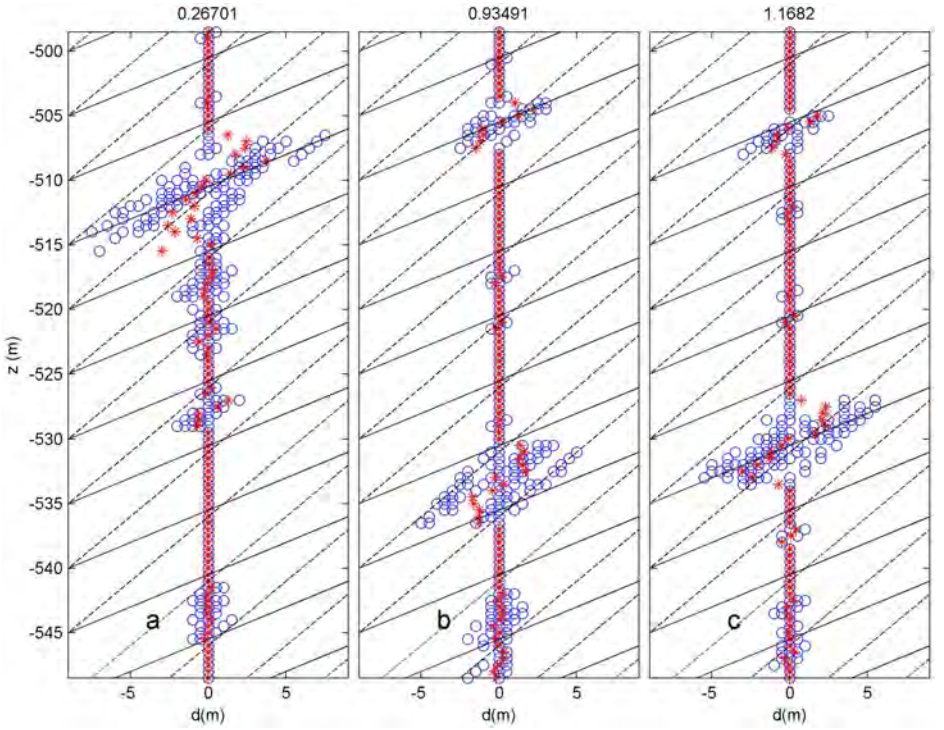

Figure 5. Ten consecutive profiles of displacements (blue circles) and their mean values at given depths (red asterisks) for t^*'s indicated above and along dashed lines in Figure 4.

The near-complete density compensation of temperature by salinity variations in combination with strong vertical turbulent activity may explain why the large "false overturn" displacement range adopts shapes that resemble those of genuine turbulent overturns, with edges aligned with $z/d = 1$ and a core of $z/d = 0.5{-}0.7$ (Fig. 7). However, in contrast with the large overturn shapes of Figure 3, the average (red asterisks) profiles do not align with $z/d = 0.5$ here. They are also more erratic; over pieces of 5–10 m, they slope $z/d \geq 1$ and regularly slope negatively in between. An exception is the lower portion of the overturn at approximately −940 m in Figure 7(b) that does slope $z/d = \sim 0.5$, but this is a genuine turbulent overturn (see Fig. 6).

As reported in van Haren and Greinert (2013), the temperature-density (referenced to 1,000 m) relationship $\delta\sigma_{1,000} = \alpha\delta\Theta$ is reasonably tight: $\alpha = -0.15 \pm 0.01$ kg m^{-3} °C^{-1}, for the second half of the thermistor string record above Opouawe Bank. The observations in Figures 6 and 7 may thus be contrasted with those of a few days later (Figs. 8 and 9). During those last 3 out of 5 days of data, genuine large turbulent overturns dominate, with a few small exceptions like the yellow arrow pointing at a bent (<10 m high) salinity intrusion

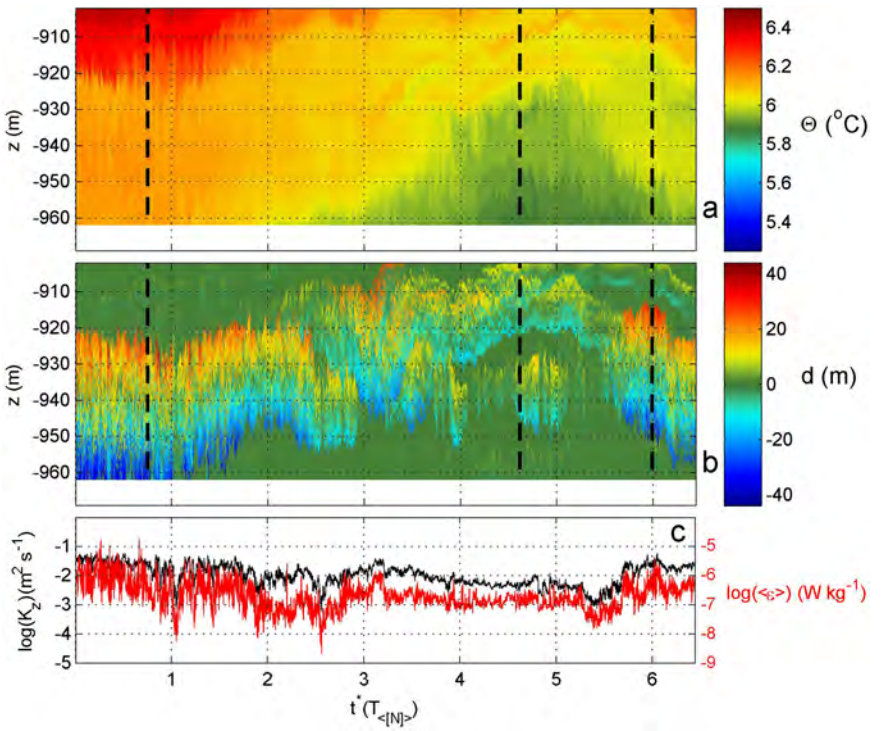

Figure 6. Overturn duration investigation for 4.8 hours between days [100.26, 100.46] of Opouawe Bank data (61 NIOZ4 sensors, none missing, at 1.0 m intervals between 7 and 67 m above the bottom) with many intrusions.

lasting $\Delta t^* \approx 1$ in Figure 8(b). The data in Figures 8 and 9 resemble the large overturns above Great Meteor Seamount (Figs. 2 and 3), even though in this example turbulence is about half as strong. The shape of the overturns is also very much alike, now with cores and average profiles aligned with slopes of 0.5–0.7 in the d-z plane, being less erratic in shape (Fig. 9). The exception of the relatively short intrusion, with main part duration of $\sim 0.5t^*$, is around midrange in Figure 9(a). As for the large persistent intrusion of Figure 7, the short intrusion shape has a mean core slope of $z/d \approx 1$.

5. Conclusions

The distinction between genuine turbulent overturns and false salinity-compensated intrusions can be easily visualized in high-resolution thermistor string data using an integrated time scaled with the local buoyancy period. The new unit, the depth-time average buoyancy period, commonly distinguishes between internal wave motions ($t^* > 1$) and turbulence ($t^* < 1$). In the present data, a train of small-scale K-H overturns is indeed found limited

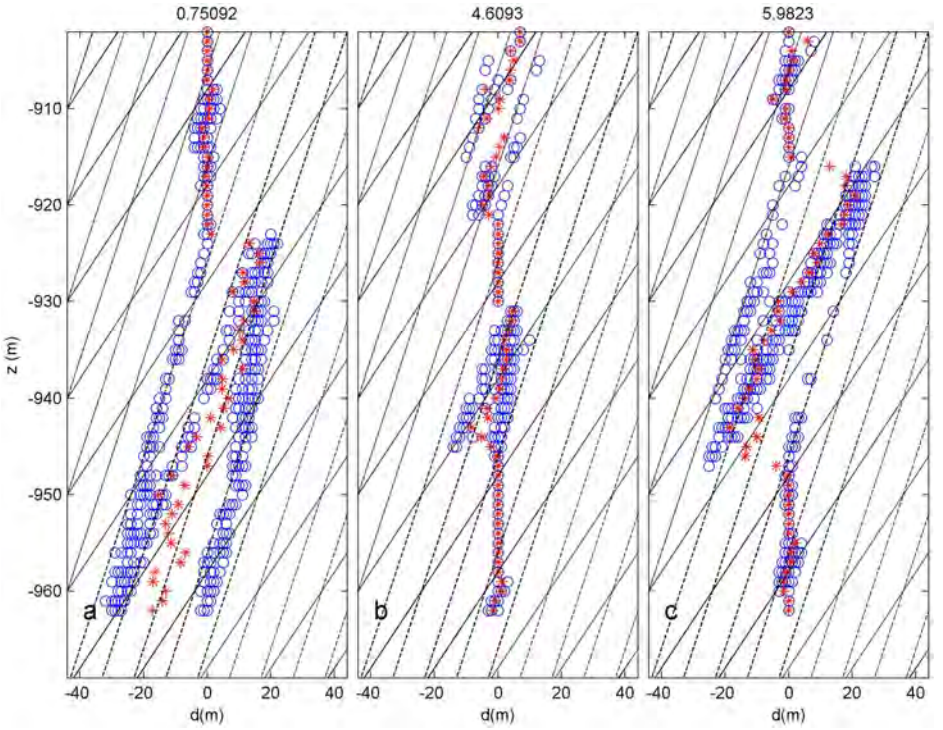

Figure 7. Ten consecutive profiles of displacements (blue circles) and their mean values at given depths (red asterisks) for t^*'s indicated above and along dashed lines in Figure 6.

by $\Delta t^* \leq 1$. In contrast, individual larger-scale, "convective" and shear-induced overturns are far from approaching this limit. Such overturns occur prior to a frontal passage and are possibly due to oblique internal wave propagation. They have $\Delta t^* = 0.3 \pm 0.1$, a value that is comparable with the timescale of growth in grid-turbulence models.

Small shear-induced K-H overturns are observed to last only $\Delta t^* = 0.03$. Because these overturns are 10 times smaller than the large overturns, it is tempting to relate $\Delta t^* \sim d \sim \varepsilon^{1/2} \sim K_z^{1/2}$ for fixed N. However, comparison of these data with those from other areas, with different N, shows ambiguous results for such a relationship, as was also concluded for N-scaling of turbulence parameters by van Haren and Gostiaux (2012). It is noted that a caveat of the present observations is their one-dimensionality in space, and future moored observations from three-dimensional arrays would be highly welcomed.

Because most intrusions could be visually detected in graphs of the scaled time axis, the additional investigation of the shape of overturns is found to be somewhat ambiguous for the present thermistor string data. K-H overturns have the best reproducible shape filling a parallelogram with sloping sides of $z/d = 1$ and long-axis slope of $z/d = 0.5$. This is

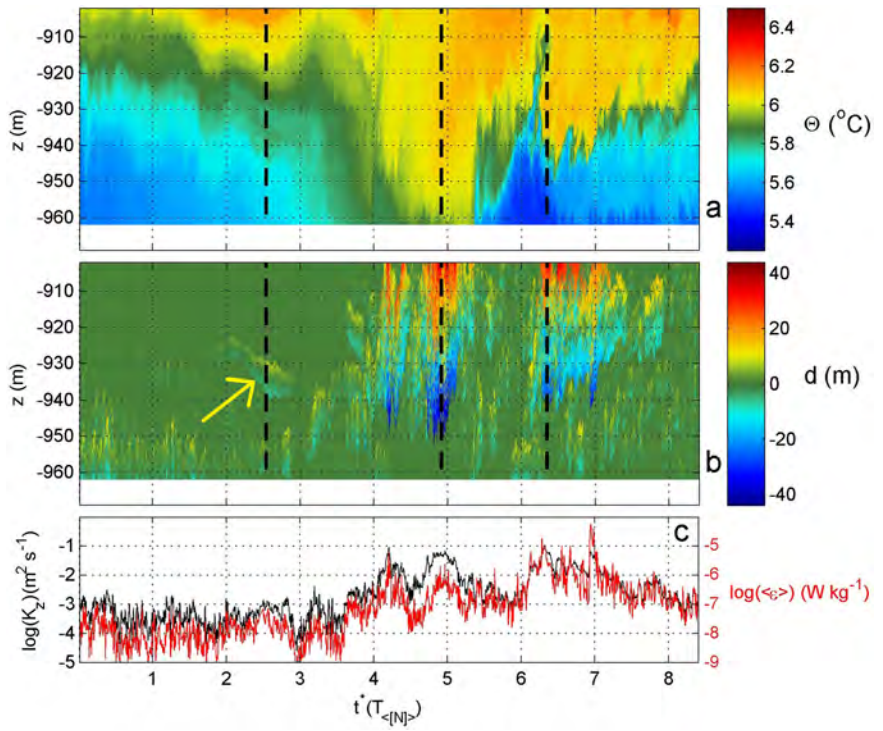

Figure 8. Overturn-duration investigation for 4.8 hours between days [103.86, 104.06] above Opouawe Bank with few salinity-compensated intrusions (except in leftmost profile, yellow arrow).

best modeled by full mixing following a solid-body overturn. Larger overturns have slopes of $z/d \approx 1$ along the sides and more erratic interior slopes, but their included smaller overturns, as in vigorous turbulence, have shapes resembling a Rankine vortex model with slopes $z/d = 0.5{-}0.7$ in the interior. Although intrusion shapes were modeled having slopes well exceeding $z/d = 1$ by van Haren and Gostiaux (2014), the presently observed intrusions have side slopes only just exceeding $z/d = 1$, together with an erratic interior. They distinguish from turbulent overturns mainly after inspection of smaller-scale pieces of 5–10 m high in the interior that slope $z/d \geq 1$ for intrusions. This partial ambiguity may be the result of the relatively coarse resolution of the thermistors in the vertical, compared with raw CTD and microstructure profiler data. It may also be attributable to the fact that the intrusions above sloping topography are likely to be mixed with genuine turbulent overturning in an area where internal wave breaking is ubiquitous. This mix results in complex overturn shapes, near-homogeneous layering in density, and, hence, near-perfect salinity compensation. It certainly provides different results from, for example, Mediterranean-outflow observations in the open ocean.

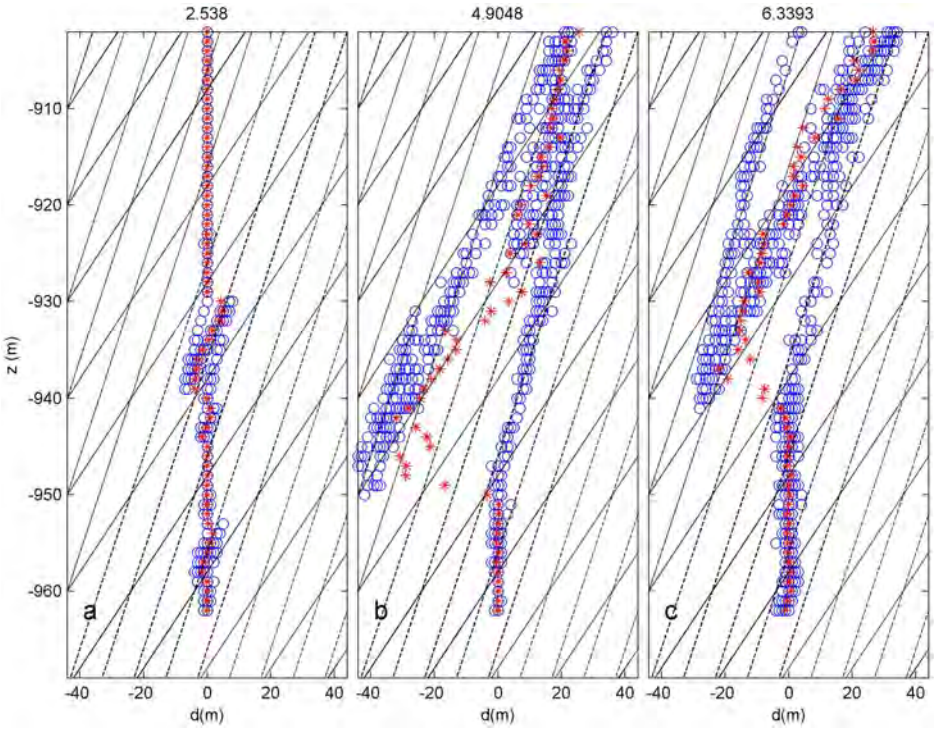

Figure 9. Ten consecutive profiles of displacements (blue circles) and their mean values at given depths (red asterisks) for t^*'s indicated above and along dashed lines in Figure 8.

Acknowledgments. The captain and crew of the R/V *Pelagia* are thanked for their pleasant cooperation during the sea operations. We acknowledge F. Mienis for overseeing the deployment and recovery of the Rockall Bank mooring. J. Greinert and the captain and crew of R/V *Sonne* are acknowledged for deployment and recovery of the Opouawe Bank mooring. We greatly thank M. Laan for design and construction of NIOZ temperature sensors and assistance in mooring preparation. The work has been financed in part by the Netherlands Organization for Scientific Research (NWO). This article was initiated during HvH's stay as visiting professor at and financed by the École Centrale de Lyon. LG was supported by the Agence Nationale de la Recherche, ANR-13-JS09-0004-01 (STRATIMIX).

APPENDIX

a. Waterfall plots of temperature and the artificial passage of shipborne CTD.

In comparison with a shipborne conductivity-temperature-depth (CTD) package, a moored NIOZ thermistor string is measuring vertical temperature-only profiles, at a rather coarse resolution of ∼1 m and relatively fast within 0.02 s irrespective of the length (up to ∼1,000 m) of the string. This quick sampling of a vertical profile is associated with the

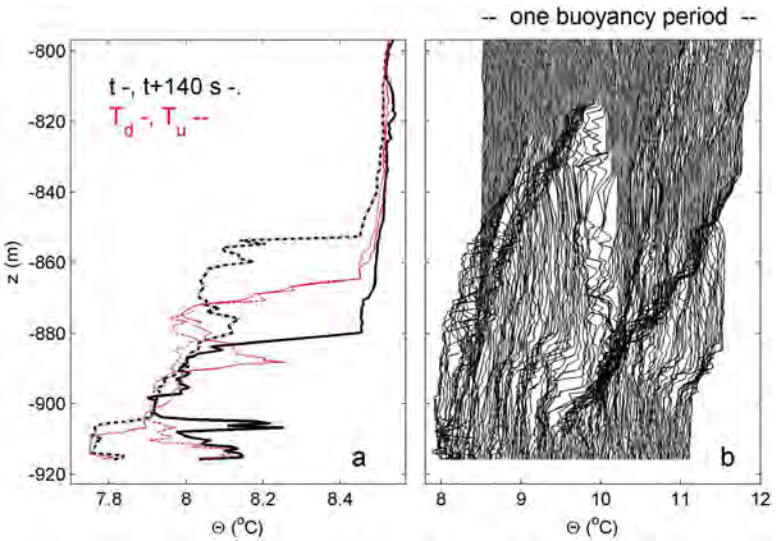

Figure A1. Vertical conservative temperature profile variations from 120 m long thermistor string above Rockall Bank (140 sensors of which 13 have been interpolated; mix of NIOZ4 and NIOZ4c sensors at 0.6 and 1.0 m intervals between 6 and 125 m above the bottom), during the passage of frontal bore (as in Fig. 1). (a) Two thermistor string profiles 140 s apart (black), compared with an artificial down- and upcast profile (red) constructed from the 1 Hz sampled thermistor string data. (b) Rudimentary scaling of time: plot of every sixth temperature profile during and after a frontal passage for a total length of time equaling the mean buoyancy period (1,950 s in this case). The temperature profiles are arbitrarily offset along the x-axis.

synchronization, which is generally done every 4 hours. To demonstrate the difference in sampling of such a string with a 24 Hz ($\sim$0.04 m vertical) sampling CTD moving at common winch speeds, we resampled some thermistor string data from the presently longest string deployed (120 m long at 55.5° N, 15.8° W; 922 m water depth above a slope of Rockall Bank, northeast Atlantic Ocean); see Figure A1. The average lowering speed of the CTD was 0.9 m s^{-1}, and the average hoisting speed 0.8 m s^{-1}, so that it would take $\sim$140 s to cover the range of thermistors.

A passage of a frontal bore, much like the one in Figure 1 but extending about two times higher, is seen to rapidly move cold water up Rockall Bank in the 140 s between the two thermistor profiles depicted (Fig. A1a). If this same passage would have been sampled by a CTD (with data averaged in 0.6 and 1.0 m vertical bins as for the thermistors), we would find either the solid red profile (for its downcast) or the dashed red profile (for its upcast). Naturally, a consecutive set of down- and upcast profiles would take twice as long, provided an immediate return at the deepest point. The individual, artificial down- and upcast profiles given here seem similar in appearance but vary considerably in the depth range of overturn displacement, quite like the two thermistor profiles.

When more thermistor string profiles are plotted, as in the waterfall plot of Figure A1(b), it is seen that the front passes much more rapidly than the local vertical-time mean buoyancy period, which spans the entire period of profiles plotted. More importantly, all overturns no matter how large, up to 70 m, have a duration of less than half the buoyancy period. It implies that they are genuine turbulent overturns. This waterfall plot is a rudimentary version of the t^* in equation (1) in which time is scaled with the local mean buoyancy period for every single 1 Hz profile.

REFERENCES

Dugan, J. P. 1984. Towed observations of internal waves and patches of fine-scale turbulence, *in* Internal Gravity Waves and Small-Scale Turbulence: Proceedings of 'Aha Huliko'a Hawaiian Winter Workshop, P. Muller and R. Pujalet, eds. Honolulu: Hawaii Institute of Geophysics, 51–64.

Gemmrich, J. R., and H. van Haren. 2001. Thermal fronts generated by internal waves propagating obliquely along the continental slope. J. Phys. Oceanogr., *31*, 649–655.

Gregg, M. C. 1987. Diapycnal mixing in the thermocline: A review. J. Geophys. Res.: Oceans, *92*, 5249–5286.

Itsweire, E. C., K. N. Helland, and C. W. Van Atta. 1986. The evolution of grid-generated turbulence in a stably stratified fluid. J. Fluid Mech., *162*, 299–338.

Marmorino, G. O. 1987. Observations of small-scale mixing processes in the seasonal thermocline. Part II: Wave breaking. J. Phys. Oceanogr., *17*, 1348–1355.

McDougall, T. J., R. Feistel, F. J. Millero, D. R. Jackett, D. G. Wright, B. A. King, G. M. Marion, C.-T. A. Chen, and P. Spitzer. 2009. Calculation of the Thermophysical Properties of Seawater: Global Ship-Based Repeat Hydrography Manual. IOCCP Report No. 14, ICPO Publication Series No. 134. Paris: UNESCO, 131 pp.

Oakey, N. S. 1982. Determination of the rate of dissipation of turbulent energy from simultaneous temperature and velocity shear microstructure measurements. J. Phys. Oceanogr., *12*, 256–271.

Osborn, T. R. 1980. Estimates of the local rate of vertical diffusion from dissipation measurements. J. Phys. Oceanogr., *10*, 83–89.

Riley, J. J., R. W. Metcalf, and M. A. Weissman. 1981. Direct numerical simulations of homogeneous turbulence in density-stratified fluids, *in* Nonlinear Properties of Internal Waves, B. J. West, ed. New York: American Institute of Physics, 79–112.

Stansfield, K., C. Garrett, and R. Dewey. 2001. The probability distribution of the Thorpe displacement within overturns in Juan de Fuca Strait. J. Phys. Oceanogr., *31*, 3421–3434.

Thorpe, S. A. 1977. Turbulence and mixing in a Scottish loch. Philos. Trans. R. Soc., A, *286*, 125–181.

———. 1987. Current and temperature variability on the continental slope. Philos. Trans. R. Soc., A, *323*, 471–517.

van Haren, H., and L. Gostiaux. 2010. A deep-ocean Kelvin-Helmholtz billow train. Geophys. Res. Lett., *37*, L03605. doi: 10.1029/2009GL041890

———. 2012. Detailed internal wave mixing above a deep-ocean slope. J. Mar. Res., *70*, 173–197.

———. 2014. Characterizing turbulent overturns in CTD-data. Dyn. Atmos. Oceans, *66*, 58–76.

van Haren, H., and J. Greinert. 2013. Variability of internal frontal bore breaking above Opouawe Bank methane seep area (New Zealand). Geochem., Geophys., Geosyst., *14*, 2460–2473. doi: 10.1002/ggge.20170

van Haren, H., M. Laan, D.-J. Buijsman, L. Gostiaux, M. G. Smit, and E. Keijzer. 2009. NIOZ3: Independent temperature sensors sampling yearlong data at a rate of 1 Hz. IEEE J. Oceanic Eng., *34*, 315–322.

Received: *16 May 2014*; revised: *9 December 2014*.